

Phase diagram and compact stars in a holographic QCD model

Luis A. H. Mamani,^{1,*} Cesar V. Flores,^{2,†} and Vilson T. Zanchin^{1,‡}

¹ *Centro de Ciências Naturais e Humanas, Universidade Federal do ABC,
Avenida dos Estados 5001, 09210-580 Santo André, São Paulo, Brazil*

² *Centro de Ciências Exatas, Naturais e Tecnológicas, UEMASUL,
Rua Godofredo Viana 1300, Centro CEP: 65901-480, Imperatriz, Maranhão, Brazil*

A holographic model is used to investigate the thermodynamics and phase the diagram of a heavy quarks system. From such a model we obtain an equation of state and explore its applicability in astrophysical conditions. For this objective, we work in the context of the Einstein-Maxwell-Dilaton (EMD) holographic model for quantum chromodynamics (QCD). At first, we show the existence of a critical point where the first-order transitions line ends, later on, we calculated an analytic expression for the equation of state. Additionally, with the aim of investigating the global properties of compact stars, such as the total gravitational mass and radius, the equation of state is used to solve the Tolman-Oppenheimer-Volkov (TOV) equations for stellar structure. The numerical results show that our equation of state is able to reproduce the expected behaviour of hybrid stars. Our main conclusion is that, by using an equation of state emerging in the framework of the EMD holographic model for QCD, it is possible to obtain quark matter properties and that it is also possible to extend the procedure to astrophysical applications.

I. INTRODUCTION

The investigation of the phase structure of quantum chromodynamics (QCD) is an open problem of modern physics and there are several research groups around the world facing this important problem. It is widely known that QCD lies in the confinement regime in the region of low temperature T and density (chemical potential μ), and that it also lies in the deconfinement regime in the region of high temperature and density. It is believed that at the boundary between these two phases, close to the chemical potential axis, there is a line describing first-order phase transitions. It is also speculated that this line terminates at the critical point, where the theory has conformal symmetry and can be described by a set of universal critical exponents. In turn, at low chemical potentials, the transition becomes crossover. Moreover, it is complicated to extract reliable information from the region where these transitions occur because QCD lies in the strong coupling regime and the usual techniques used in perturbative QCD do not work. On the other hand, it is known that lattice QCD provides reliable results at zero chemical potential (in the strong coupling regime), however, it does not work when finite chemical potential effects are considered. Among other problems arising at finite density is the sign problem. Nevertheless, most of the relevant problems of modern physics are related to QCD at finite density, for example, heavy-ion collisions and investigation of compact objects in astrophysics. In the last years, lattice QCD is overcoming the application problems by implementing new techniques, but these do work in the regime of small chemical potentials and no

reliable results at large densities are available so far, see e.g. [1–3] for a review.

Another theoretical framework for investigating QCD-like theories at finite temperature and density has been implemented following the holographic principle [4, 5]. The anti-de Sitter/conformal field theory (AdS/CFT) correspondence [6–8], which is a realization of the holographic principle, allows us to investigate the duality between a strongly coupled field theory living in a d -dimensional spacetime and its dual gravitational theory (in principle quantum gravity) living in a $(d + 1)$ -dimensional spacetime. The duality arising directly from superstring theory in ten or eleven spacetime dimensions is known in the literature as a top-down approach, see for instance Ref. [9–11]. On the other hand, the bottom-up approach relates quantum field theories living in four-dimensional spacetimes with a dual classical gravitational theory living on five-dimensional anti-de Sitter spacetime. These models have phenomenological motivations and are build using phenomenological results in the quantum field theory side. In the first stages the backreaction on the gravitational background was neglected [12–14], then, the backreaction is considered [15–22], this approach is also known as holographic QCD. In the context of holographic QCD models it was shown that scenarios with simple gravitational theories in five-dimensional spacetime are able to mimic certain properties of QCD, like the equation of state [23, 24] and the thermodynamics of the gluon plasma [25–29]. What is interesting is that these results were obtained with a gravitational action coupled to a scalar field. The conformal symmetry breaking is realized by the nontrivial profile of the scalar field. In the same way, by adding an additional U(1) gauge field in the gravitational action we include finite chemical potential for baryon number. Thus, the gauge field in the five-dimensional theory is dual to the baryon density current and it may be generated turning on an electric field in the gravitational background. It is worth

*Electronic address: luis.mamani@ufabc.edu.br

†Electronic address: cesar.vasquez@uemasul.edu.br

‡Electronic address: zanchin@ufabc.edu.br

mentioning that the metric is asymptotically Reissner-Nordström AdS metric.

Previous works investigated the phase structure and critical point using holographic QCD at finite temperature and density [30–39]. It is worth pointing out that in [30, 31] the authors found a phase diagram in agreement with that is expected in QCD, they also found a critical point. Interestingly, the information concerning the quarks seems to be codified in the gauge field and a scalar function, gauge kinetic function, which characterizes the non-minimal coupling between the dilaton and gauge field. It is also interesting to point out that the authors of Ref. [33] investigated a holographic model for heavy quarks, which phase diagram differs from the one obtained in [30, 31]. Phenomenological properties, like mesons dissociation, were also investigated using holographic models, see for instance Refs. [40–43].

On the other hand, recently the interest in investigating neutron stars increased promoted by the results collected by the LIGO and VIRGO collaborations [44]. Previous investigations of compact objects, like neutron stars, were developed using the Tolman [45] and Oppenheimer-Volkov [46] equations. A pivotal point to solve these equations is the equation of state (EoS) of matter in the interior of these objects, where it is under extreme conditions. The results obtained applying usual methods in perturbative QCD, for example, are not reliable because of the high density and strong coupling. It is also believed that the collision of neutron stars will constraint, even more, the EoS in such extreme conditions. At this point, the holographic approach seems to be useful for investigating the nuclear matter in such conditions. As mentioned above, this theoretical framework maps the problem into a dual classical gravitational theory, where, in principle, we can face the problem using techniques available in the literature. This way to face the problem will allow us to shed new light in the understanding of compact objects, like neutron, quark matter, or even hybrid stars.

In this paper, we work with the holographic model proposed in Ref. [17] (see Appendix G), then applied it to investigate Yang-Mills theories at finite temperature in Ref. [47]. To include finite chemical potential effects in the dual field theory we add an abelian gauge field in the five-dimensional action following Refs. [30, 31]. Thus, the holographic model describes the heavy quarks system in the dual field theory [33]. One of the aims of this work is to apply our equation of state to solve the Tolman-Oppenheimer-Volkov-(TOV) equations in order to investigate the behavior of the mass vs radius relationship for hybrid stars. As far as we know previous works in the literature have investigated the internal structure of stars using holography, see for instance Refs. [48–56]. The advantage of working with the model of Ref. [47] is that we get analytic solutions for some of the thermodynamic variables like the temperature and entropy.

The paper is organized as follows. In Section II we introduce the five-dimensional model. We also solve the

Einstein-Maxwell-Dilaton equations using a simple holographic model and get an analytic expression for the gauge field, temperature, and entropy. The asymptotic analysis of the thermodynamic variables allows us to get an analytic equation of state. In the end, we investigate the extremal solution, i.e., when the temperature vanishes. In Section III, our numerical results are presented and discussed. Section IV is devoted to investigating the phase structure of the holographic model. In Section V we implement the matching procedure between the nuclear EoSs and the quark matter EoS, and then we solve the Tolman-Oppenheimer-Volkov equations to get the mass-radius relationship. Finally, we conclude and discuss future extensions of the present work in Section VI. Complementary material is left in Appendix A.

II. THE FIVE-DIMENSIONAL EMD MODEL

A. The five-dimensional background

The gravitational dual of the Yang-Mills theory in four-dimensional spacetime is described by a five-dimensional gravitational theory whose action contains the metric coupled to a scalar field and, in order for including finite density effects in the dual field theory, a gauge field must be added in the five-dimensional action, and thus the metric is also coupled to this field. The most general five-dimensional action is defined by [30]

$$S = \frac{1}{2\kappa^2} \int dx^5 \sqrt{-g} [R + \mathcal{L}], \quad (1)$$

where the Lagrangian is given by

$$\mathcal{L} = -\frac{4}{3}(\partial^m \Phi)(\partial_m \Phi) + V(\Phi) - \frac{f_\Phi(\Phi)}{4} F^{mn} F_{mn}, \quad (2)$$

where Φ is the dilaton field, $V(\Phi)$ is the dilaton potential and contains the cosmological constant term, $-6/\ell^2$, where ℓ is the AdS radius, F_{mn} the gauge field defined by $F_{mn} = \partial_m A_n - \partial_n A_m$ and κ is the Newton constant in five-dimensional spacetime, while $f_\Phi(\Phi)$ is the gauge kinetic function, which includes the non-minimal coupling between the dilaton and gauge field. In the present work we restrict ourselves to the case $f_\Phi(\Phi) = 1$. The equations of motion obtained from varying the action (1) are:

$$\begin{aligned} G_{mn} - \frac{4}{3}(\partial_m \Phi)(\partial_n \Phi) + \frac{2g_{mn}}{3}(\partial^p \Phi)(\partial_p \Phi) - \frac{g_{mn}}{2}V(\Phi) \\ + \frac{1}{2} \left(\frac{g_{mn}}{4} F^{pq} F_{pq} - g^{pq} F_{nq} F_{mp} \right) = 0, \end{aligned} \quad (3)$$

where G_{mn} is the Einstein tensor. In turn, the Maxwell equations are:

$$\partial_m (\sqrt{-g} g^{mp} g^{nq} F_{pq}) = 0. \quad (4)$$

Finally, the Klein-Gordon equation

$$\frac{8}{3\sqrt{-g}}\partial_m(\sqrt{-g}\partial^m\Phi) + \partial_\Phi V(\Phi) = 0. \quad (5)$$

In applications of holographic QCD it is usual to consider an ansatz on the metric tensor and gauge field of the form [40, 41]

$$ds^2 = e^{2A} \left(-f(z)dt^2 + \frac{1}{f(z)}dz^2 + dx_i dx^i \right), \quad (6)$$

$$A_0 = A_0(z), \quad A_1 = A_2 = A_3 = A_4 = 0,$$

where A is the warp factor, we also define the new function $\zeta = e^{-A}$ to rewrite the equations of motion. Neglecting the dilaton field, the solution of the Einstein-Maxwell equations is the Reissner-Nordström AdS black hole (RNAdS). Following the convention of Refs. [38, 41, 42]) we are going to consider the constant κ given by

$$\frac{1}{\kappa^2} = \frac{N_c^2}{(2\pi)^2 \ell^3}, \quad (7)$$

where N_c is the number of colors. Plugging the ansatz (6) in (3) we get the following system of coupled differential equations:

$$\begin{aligned} \frac{\zeta''}{\zeta} - \frac{4}{9}(\Phi')^2 &= 0, \\ f'' - \frac{3\zeta'}{\zeta}f' - (\zeta A_0')^2 &= 0, \\ 3\zeta'' - 12\frac{\zeta'^2}{\zeta} + \frac{3f'\zeta'}{f} + \frac{2V - \zeta^4(A_0')^2}{2f\zeta} &= 0, \end{aligned} \quad (8)$$

where the primes stand for total derivatives with respect to the variable z , d/dz . As can be seen, these equations involve the warp factor, dilaton field and its potential, horizon function, and the gauge field. On the other hand, the Maxwell equation is obtained plugging (6) in (4)

$$\left(\frac{A_0'}{\zeta} \right)' = 0, \quad (9)$$

which solution is given by $A_0' = c_1 \zeta(z)$, where c_1 is the integration constant. The complete solution of the gauge field is given by

$$A_0(z) = c_2 + c_1 \int_z dx \zeta(x). \quad (10)$$

B. The holographic model

Once we get the equations of motion we would like to find solutions. In the following we introduce the holographic model we are going to work with, the model originally proposed in Ref. [17] (see Appendix G) was used to investigate confinement properties of $SU(N)$ Yang-Mills

theories in Ref. [47]. In the holographic model, the warp factor is given by

$$\zeta(z) = \frac{z}{\ell} e^{\Lambda^2 z^2}, \quad (11)$$

where Λ is a parameter. Our motivation is the same as in Ref. [47], even though we do not know the explicit form of the dilaton potential, the model allows us to investigate the general properties of the dual field theory in the strong coupling regime. Plugging (11) in (10) the integration gives us

$$A_0(z) = c_2 + \frac{c_1}{\ell} \frac{(e^{\Lambda^2 z^2} - 1)}{2\Lambda^2}. \quad (12)$$

We may fix the constants c_1 and c_2 by comparing the asymptotic form of (12) close to the boundary with the corresponding Reissner-Nordström AdS (RNAdS) solution, which takes the form $A_0 = \mu - Qz^2 + \dots$ [38, 41, 42]), thus, we get $c_2 = \mu$ and $c_1 = -2\ell Q$. Hence, the gauge field is given by

$$A_0(z) = \mu + \frac{Q}{\Lambda^2} \left(1 - e^{\Lambda^2 z^2} \right), \quad (13)$$

where μ is the chemical potential and Q a parameter related to the charge of the black hole. The gauge field should be regular at the horizon, i.e., $A_0(z_h) = 0$, this condition allows us to find a relation between Q and μ

$$Q = \frac{\Lambda^2 \mu}{e^{\Lambda^2 z_h^2} - 1}. \quad (14)$$

Plugging (14) in (13) we get the analytic solution for the gauge field

$$A_0(z) = \mu \frac{e^{\Lambda^2 z^2} - e^{\Lambda^2 z_h^2}}{1 - e^{\Lambda^2 z_h^2}}, \quad (15)$$

from the expansion of this result close to the boundary we read off the baryon density $A_0 = \mu + 2\Lambda^2 \mu z^2 / (1 - e^{\Lambda^2 z_h^2}) + \dots$,

$$\rho = -\frac{\Lambda^2 \mu}{1 - e^{\Lambda^2 z_h^2}}. \quad (16)$$

Thus, the relation between the parameter Q and baryon density is $\rho = Q$ [33]. On the other hand, plugging (11) and (13) in the second equation of (8) we get a differential equation for the horizon function, which solution is given by

$$f = c_4 + \frac{c_3 e^{3\Lambda^2 z^2} (3\Lambda^2 z^2 - 1)}{18\Lambda^4} + \frac{Q^2 e^{4\Lambda^2 z^2} (4\Lambda^2 z^2 - 1)}{16\ell^2 \Lambda^6}, \quad (17)$$

we fix the remaining constants c_3 and c_4 with the conditions $f(0) = 1$ and $f(z_h) = 0$. Hence, they are given

by

$$c_3 = -\frac{144\ell^2\Lambda^6 + 9Q^2 \left[1 + e^{4\Lambda^2 z_h^2} (4\Lambda^2 z_h^2 - 1)\right]}{8\ell^2\Lambda^2 (1 + e^{3\Lambda^2 z_h^2} (3\Lambda^2 z_h^2 - 1))},$$

$$c_4 = \frac{e^{3\Lambda^2 z_h^2} (16\ell^2\Lambda^6 + Q^2) (3\Lambda^2 z_h^2 - 1)}{16\ell^2\Lambda^6 (1 + e^{3\Lambda^2 z_h^2} (3\Lambda^2 z_h^2 - 1))} + \frac{Q^2 e^{4\Lambda^2 z_h^2} (1 - 4\Lambda^2 z_h^2)}{16\ell^2\Lambda^6 (1 + e^{3\Lambda^2 z_h^2} (3\Lambda^2 z_h^2 - 1))}. \quad (18)$$

The relation between Q and q is obtained by expanding Eq. (17) close to the boundary where this expression reduces to the RNAdS solution, thus, we get

$$Q^2 = 3\ell^2 q^2, \quad (19)$$

where q is the charge of the black hole. It is worth mentioning that taking the limit of zero Λ Eq. (17) reduces to

$$f(z) = 1 - \left(\frac{1}{z_h^4} + q^2 z_h^2\right) z^4 + q^2 z^6, \quad (20)$$

which is the horizon function of the RNAdS black hole solution. On the other hand, expanding Eq. (17) close to the boundary, i.e., small z_h and z , we obtain

$$f = 1 + \left(-\frac{1}{z_h^4} + \frac{2\Lambda^2}{z_h^2} - q^2 z_h^2 + \mathcal{O}(z_h^3, \Lambda^4)\right) z^4 + \left(q^2 - \frac{2\Lambda^2}{z_h^4} + \frac{4\Lambda^4}{z_h^2} + \mathcal{O}(z_h^3, \Lambda^6)\right) z^6 + \mathcal{O}(z^7), \quad (21)$$

where $\mathcal{O}(\Lambda, z_h)$ are subleading contributions. Interestingly, in the limit of zero Λ we recover the RNAdS solution. Then, we may see this equation as a deformed RNAdS black hole solution.

On the other hand, the dilaton may be obtained plugging (11) into the first equation of (8), then, the dilaton takes the form [17]

$$\Phi = \frac{3z}{4} \sqrt{6\Lambda^2 + 4z^2\Lambda^4} + \frac{9}{4} \ln \left[\frac{2z\Lambda^2 + \sqrt{6\Lambda^2 + 4z^2\Lambda^4}}{\sqrt{6\Lambda^2}} \right]. \quad (22)$$

Expanding the last result close to the boundary we get

$$\Phi = \phi_1 z + \phi_3 z^3 + \dots, \quad (23)$$

where $\phi_1 = 3\Lambda/\sqrt{6}$ is interpreted as the source, while $\phi_3 = \Lambda^3/\sqrt{6}$ as the vacuum expectation value in the dual field theory. Then, Φ is dual to an operator of dimension $\Delta = 3$. In turn, the dilaton potential may be calculated from the last equation of (11), plugging the analytical solutions of the background equations and expanding close to the boundary

$$V = \frac{12}{\ell^2} + \frac{54\Lambda^2 z^2}{\ell^2} + \dots \quad (24)$$

writing in terms of the dilaton field the potential becomes

$$V = \frac{12}{\ell^2} - \frac{4}{3} M_\Phi^2 \Phi^2 + \dots, \quad (25)$$

where $M_\Phi^2 \ell^2 = \Delta(\Delta - 4)$ is the mass of the dilaton field. Setting $\Delta = 3$ we recover (24), showing the consistency of the expansion (23).

C. Thermodynamics

The knowledge of the horizon function allows the calculation of the Hawking temperature, which is defined by

$$T = -\frac{1}{4\pi} \partial_z f(z) \Big|_{z=z_h}. \quad (26)$$

As the holographic model we are working with presents an analytic expression for the warp factor, the expression of the temperature reads as

$$T = \frac{3z_h^3 e^{3\Lambda^2 z_h^2} \left[48\Lambda^6 - q^2 \left(16e^{\Lambda^2 z_h^2} + e^{4\Lambda^2 z_h^2} (12\Lambda^2 z_h^2 - 7) - 9\right)\right]}{32\pi\Lambda^2 \left[1 + e^{3\Lambda^2 z_h^2} (3\Lambda^2 z_h^2 - 1)\right]}. \quad (27)$$

The dependence on the chemical potential is obtained plugging (19) and (14) in (27). A plot of the temperature for different values of the chemical potential is displayed in Fig. 1, where we can see that the temperature has

different branches depending on the value of the chemical potential. Therefore, must be a value of the chemical potential where the temperature becomes a monotonic decreasing function, we call this value as μ_c . This value

may be calculated by solving the equation $\partial_{z_h} T = \partial_{z_h}^2 T$, which is the place where there is no maximum either minimum in Fig. 1.

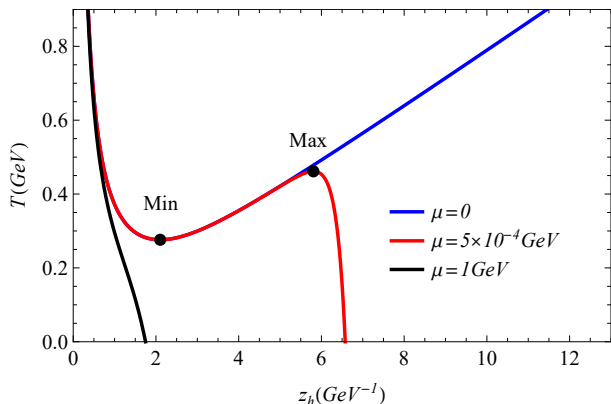


FIG. 1: The figure shows the temperature for different values of the chemical potential, while the other parameters are: $\kappa = 2\pi/N_c$, with $N_c = 3$ and $\Lambda = 0.4\text{GeV}$.

Still concerning to Fig. 1, for $\mu = 5 \times 10^{-4}$ GeV there is a minimum and maximum in the temperature, the branch belonging to this region $z_{\text{Min}} < z_h < z_{\text{Max}}$ represents an unstable phase where the specific heat becomes negative, as we shall see below.

On the other hand, to calculate the equation of state we first calculate the entropy through the Bekenstein-Hawking formula

$$S = \frac{\mathcal{A}}{4G_5} = \frac{2\pi V_3}{\kappa^2 \zeta^3(z_h)} \quad (28)$$

where \mathcal{A} is the transverse area and V_3 is the three-dimensional space volume. Plugging (11) in the last expression we get the entropy density ($s = S/V_3$)

$$s = \frac{2\pi\ell^3}{\kappa^2 z_h^3} e^{-3\Lambda^2 z_h^2}. \quad (29)$$

So far we have calculated the temperature and entropy density as a function of $s(z_h, \mu)$. In turn, the first law of thermodynamics in the presence of chemical potential may be rewritten as [30]

$$d\mathcal{F} = -s dT - \rho_N d\mu, \quad (30)$$

where \mathcal{F} is the free energy density and $\rho_N = N/V$ the number density. The pressure is given by

$$p = -\mathcal{F}, \quad (31)$$

while the free energy may be calculated through the relation

$$\mathcal{F} = \int_{z_h}^{\infty} s(\tilde{z}_h) \left(\frac{dT(\tilde{z}_h)}{d\tilde{z}_h} \right) d\tilde{z}_h. \quad (32)$$

In the last expression we implicitly imposed the condition that the free energy in the limit of infinity z_h , i.e., the

free energy of the thermal gas, is zero [33]. Once we get the free energy we know the pressure, which is given by Eq. (31), while the energy density is calculated through the thermodynamic relation $\epsilon = \mathcal{F} + Ts + \mu\rho$.

D. Asymptotic analysis

Let us calculate the asymptotic behavior of the thermodynamic variables. In this section we work on the branch where there are no instabilities, i.e., close to the boundary, see Fig. 1. Then, expanding Eq. (27) close to the boundary (which means that we are considering the big black holes branch) and plugging the relation (19) the temperature becomes

$$T = \frac{1}{\pi z_h} + \frac{\Lambda^2 z_h}{\pi} + \frac{\Lambda^4 z_h^3}{4\pi} - \left(\frac{q^2}{2\pi} + \frac{\Lambda^6}{20\pi} \right) z_h^5 + \mathcal{O}(z_h^7). \quad (33)$$

It is worth mentioning that in the limit of vanishing Λ we recover the RNAdS expression for the temperature. One more interesting relationship is the one relating the temperature and chemical potential, which is obtained plugging (14) and (19) in (27), then, expanding close to the boundary

$$T = \frac{1}{\pi z_h} + \left(\frac{\Lambda^2}{\pi} - \frac{\mu^2}{6\ell^2} \right) z_h + \left(\frac{\Lambda^4}{4\pi} - \frac{3\Lambda^2 \mu^2}{8\pi\ell^2} \right) z_h^3 - \left(\frac{\Lambda^6}{20\pi} + \frac{151\Lambda^4 \mu^2}{360\pi\ell^2} \right) z_h^5 + \mathcal{O}(z_h^7). \quad (34)$$

The RNAdS solution is obtained by setting Λ to zero and replacing $\mu/z_h^2 = Q$. Now, we may invert the asymptotic series (34) such that the expression for z_h becomes

$$z_h = \frac{1}{\pi T} + \left(\frac{\Lambda^2}{\pi^3} - \frac{\mu^2}{6\pi^3\ell^2} \right) \frac{1}{T^3} + \mathcal{O}(1/T^5). \quad (35)$$

This result will be useful when we calculate the thermodynamic variables as a function of the chemical potential and temperature.

Let us calculate asymptotic expressions for the baryon density, entropy, and free energy density close to the boundary, i.e., in the high-temperature regime. Then, plugging (35) in (16) we get

$$\rho = \frac{\mu^3}{3\ell^2} - \frac{5\Lambda^2 \mu}{2} + \pi^2 T^2 \mu + \mathcal{O}(\Lambda^4 \mu/T^2). \quad (36)$$

Whereas the entropy density, Eq. (29), becomes

$$s = \frac{2\pi^4 \ell^3 T^3}{\kappa^2} + \frac{\pi^2 \ell (\mu^2 - 12\Lambda^2 \ell^2) T}{\kappa^2} + \mathcal{O}(\Lambda^4/T, \Lambda^2 \mu^2/T, \mu^4/T). \quad (37)$$

In turn, the free energy density (32) is given by

$$\mathcal{F} = -\frac{\pi^4 \ell^3 T^4}{2\kappa^2} + \frac{\pi^2 \ell}{6\kappa^2} (36\Lambda^2 \ell^2 - 7\mu^2) T^2 - \frac{9\ell^3 \Lambda^4}{\kappa^2} + \frac{10\ell \Lambda^2 \mu^2}{3\kappa^2} - \frac{11\mu^4}{36\kappa^2 \ell} + \dots, \quad (38)$$

while the pressure is the negative of the free energy. It is worth pointing out that the free energy (38) splits out in a piece depending on the temperature, another depending on the chemical potential and the last one depending on a mixture. Following an argument similar to the one of Ref. [53] (see also [54]), neglecting the piece depending on the temperature, then, we may calculate an equation of state, which does not depend on the temperature. Thus, the free energy we are going to work with is given by

$$\mathcal{F} = -\frac{11\mu^4}{36\kappa^2\ell} + \frac{10\ell\Lambda^2\mu^2}{3\kappa^2} - \frac{9\ell^3\Lambda^4}{\kappa^2}. \quad (39)$$

It is worth mentioning that we do not impose any condition on μ and Λ to get this result. The free energy has the same mathematical structure as one expression proposed in Ref. [58], where the authors used a phenomenological construction to investigate the quark matter stars. Hence, the results we obtain support the heavy quarks interpretation we are considering in this work. In turn, the pressure is given by

$$p = \frac{11\mu^4}{36\kappa^2\ell} - \frac{10\ell\Lambda^2\mu^2}{3\kappa^2} + \frac{9\ell^3\Lambda^4}{\kappa^2}. \quad (40)$$

Then, at large densities the energy density is obtained using $\epsilon = \mu\partial_\mu p - p$,

$$\epsilon = \frac{11\mu^4}{12\kappa^2\ell} - \frac{10\ell\Lambda^2\mu^2}{3\kappa^2} - \frac{9\ell^3\Lambda^4}{\kappa^2}, \quad (41)$$

rewriting the last expression as a function of the pressure

$$\epsilon = 3p + \frac{40\ell^{3/2}\Lambda^2\sqrt{11\kappa^2p + \ell^3\Lambda^4}}{11\kappa^2} + \frac{4\ell^3\Lambda^4}{11\kappa^2}. \quad (42)$$

So far, we do not impose any restrictions on the chemical potential, i.e., if it is large or small. Expanding (42) in the regime of high pressures.

$$\epsilon = 3p + \frac{40\ell^{3/2}\Lambda^2}{\sqrt{11}\kappa}\sqrt{p} + \frac{4\ell^3\Lambda^4}{11\kappa^2} + \mathcal{O}(1/\sqrt{p}). \quad (43)$$

It is worth mentioning that Eq. (43) has the same mathematical form, unless the constant, that the equation of state obtained in the holographic model of Ref. [53].

E. Extremal solution

In the previous section we have calculated an analytic equation of state by approximating the thermodynamics variables close to the boundary, i.e., in the high-temperature regime. However, from a pragmatic point of view, it is more convenient to find out an equation of state in the zero temperature case. A way for reaching this requirement in the holographic model is to consider the extremal solution. This solution is obtained when the Hawking temperature (27) vanishes. Hence, by solving

the equation $T = 0$ we may express the parameter q as a function of Λ and z_h in the form

$$q = \frac{4\sqrt{3}\Lambda^3}{(-9 + 16e^{\Lambda^2 z_h^2} + e^{4\Lambda^2 z_h^2}(12\Lambda^2 z_h^2 - 7))^{1/2}}. \quad (44)$$

The relation between the chemical potential μ , Λ , and z_h in the extremal case is obtained by plugging relation (44) in (19),

$$\mu = \frac{12\ell\Lambda\left(e^{\Lambda^2 z_h^2} - 1\right)}{(-9 + 16e^{\Lambda^2 z_h^2} + e^{4\Lambda^2 z_h^2}(12\Lambda^2 z_h^2 - 7))^{1/2}}, \quad (45)$$

where Eq. (14) was also employed. It is convenient to get a relation of z_h as a function of the chemical potential, for that reason we may expand the last equation close to the boundary, i.e., $z_h = 0$,

$$\mu = \frac{\sqrt{6}\ell}{z_h} - \frac{5\sqrt{6}\ell\Lambda^2 z_h}{8} + \frac{149\ell\Lambda^4 z_h^3}{320\sqrt{6}} + \mathcal{O}(z_h^5) \quad (46)$$

Inverting the last asymptotic series we get

$$z_h = \frac{\sqrt{6}\ell}{\mu} - \frac{15\sqrt{6}\ell^3\Lambda^2}{4\mu^3} + \mathcal{O}(1/\mu^5). \quad (47)$$

Then, plugging (47) in (29) we get the entropy. However, as one of the aims of this paper is to get an analytic equation of state we expand the entropy in the region of large densities, this approximation gives us the result

$$s = \frac{\pi\mu^3}{3\sqrt{6}\kappa^2} - \frac{3\sqrt{6}\pi\ell^2\Lambda^2\mu}{8\kappa^2} + \frac{159\sqrt{6}\pi\ell^4\Lambda^4}{16\kappa^2\mu} + \mathcal{O}(1/\mu^3) \quad (48)$$

In the regime of large densities terms depending on $\mathcal{O}(1/\mu)$ may be neglected. We observe that Eq. (48) in the Λ zero limit reduces to the RNAdS extremal result, cf. (A15) in Appendix A. The subleading terms in Eq. (48) may be interpreted as deformations of the RNAdS extremal solution. Implementing the same procedure for the free energy we get

$$\mathcal{F} = -\frac{\mu^4}{12\ell\kappa^2} - \frac{75\ell^3\Lambda^4}{32\kappa^2} + \mathcal{O}(\log(\sqrt{6}\ell/\mu), 1/\mu^2). \quad (49)$$

The pressure is given by $p = -\mathcal{F}$. It is worth mentioning that in the Λ zero limit we recover the RNAdS extremal solution, see Eq. (A15) in Appendix A. In turn, the equation of state is given by

$$\epsilon = 3p - \frac{75\ell^3\Lambda^4}{8\kappa^2}. \quad (50)$$

The subleading term may be interpreted as a deformation of the conformal theory, which equation of state is given by $\epsilon = 3p$.

To finish this section we are going to rewrite the metric (6) close to the horizon. Then, expanding the horizon function (17) becomes

$$f \approx \mathcal{K} \left(12\frac{\tilde{z}^2}{z_h^2} + (28 + 56z_h^2\Lambda^2)\frac{\tilde{z}^3}{z_h^3} + \mathcal{O}(\tilde{z}^4/z_h^4) \right), \quad (51)$$

where $\tilde{z} = z - z_h$, the constant \mathcal{K} is given by

$$\mathcal{K} = \frac{24\Lambda^6 z_h^6 e^{4z_h^2\Lambda^2}}{-9 + 16e^{z_h^2\Lambda^2} + e^{4z_h^2\Lambda^2} (12z_h^2\Lambda^2 - 7)}. \quad (52)$$

Then, close to the horizon the metric becomes

$$ds^2 = -12 \frac{\mathcal{K} e^{-z_h^2\Lambda^2} \ell^2 \tilde{z}^2}{z_h^4} dt^2 + \frac{\ell^2 e^{-z_h^2\Lambda^2}}{12\mathcal{K}\tilde{z}^2} d\tilde{z}^2 + \frac{\ell^2 e^{-z_h^2\Lambda^2}}{z_h^2} dx_i dx^i. \quad (53)$$

Finally, after defining the new variable $\tilde{z} = \hat{r} z_h^2 / \ell^2$ the last equation reads

$$ds^2 = -12 \frac{\mathcal{K} e^{-z_h^2\Lambda^2} \hat{r}^2}{\ell^2} dt^2 + \frac{\ell^2 e^{-z_h^2\Lambda^2}}{12\mathcal{K}\hat{r}^2} d\hat{r}^2 + \frac{\ell^2 e^{-z_h^2\Lambda^2}}{z_h^2} dx_i dx^i. \quad (54)$$

The point is that in the limit of zero Λ , $\mathcal{K} = 1$ and the metric (54) reduces to the $AdS_2 \times \mathbb{R}^3$ (see Appendix A). The emergence of this geometry is related to the emergence of quantum criticality in the dual field theory [57]. Hence, we may interpret the metric (54) as a deformation of the $AdS_2 \times \mathbb{R}^3$ geometry due to the presence of the parameter Λ .

III. THERMODYNAMICS: NUMERICAL RESULTS

Here we calculate the thermodynamic variables by means of numerical methods and show the main results in a set of graphs.

Figure 2 shows a plot of s/T^3 as a function of the temperature for different values of the chemical potential. For $\mu = 5 \times 10^{-4} \text{ GeV}$ (blue line) we can see that s/T^3 starts to grow up above T_c , besides that, s/T^3 approaches to the conformal limit in the high temperature regime. For $\mu = \mu_c = 0.095 \text{ GeV}$ (red dashed line), s/T^3 starts to grow up at $T = T_c$, approaching asymptotically to the conformal limit for high temperatures. For $\mu = 0.15 \text{ GeV}$ (black line), s/T^3 starts to grow up below T_c , approaching asymptotically to the conformal limit for high temperatures.

The free energy density is displayed in the top panel of Fig. 3, as can be seen, for $\mu < \mu_c$ (blue line) it becomes a multi-valued function, which may be interpreted as the transition between two phases, this feature is a characteristic signal of the first-order phase transition. In turn, in the case, $\mu = \mu_c$ (red line) the free energy becomes a decreasing function up to reach the point (T_c, \mathcal{F}_c) , where the derivative is not defined, this is the critical point. Meanwhile, for $\mu > \mu_c$ the free energy becomes a smooth decreasing function, which may be interpreted as the stable phase where crossover transitions occur.

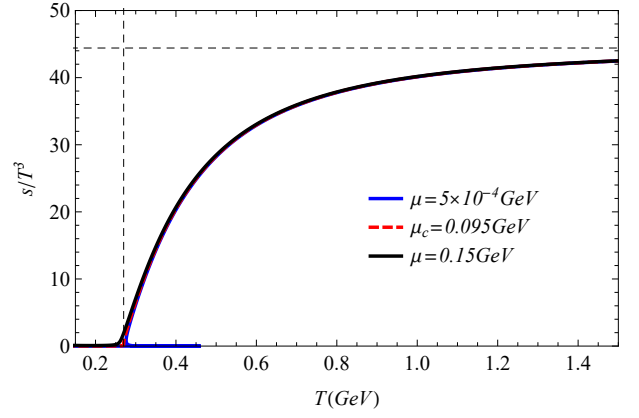


FIG. 2: The figure shows s/T^3 as a function of the temperature for different values of the chemical potential. We observe that the values asymptotically approach to the conformal value, horizontal dashed line, $s/T^3 = \pi^2 \ell^2 N_c^2 / 2$, where we have set $N_c = 3$ and $\Lambda = 0.4 \text{ GeV}$. Vertical line represents $T = 0.270 \text{ GeV}$.

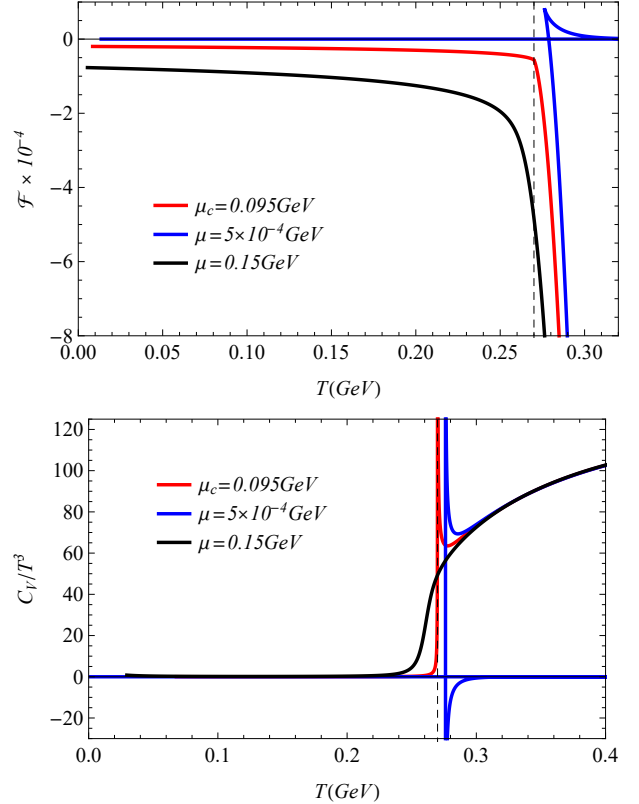


FIG. 3: Top: The figure shows the free energy as a function of the temperature for different values of the chemical potential: $\mu < \mu_c$ (blue line), $\mu = \mu_c$ (red line) and $\mu_c < \mu$ (black line). Bottom: The figure shows the specific heat as a function of the temperature for different values of the chemical potential: $\mu < \mu_c$ (blue line), $\mu = \mu_c$ (red line) and $\mu_c < \mu$ (black line). In both figures, the vertical line represents $T = 0.270 \text{ GeV}$.

In turn, the specific heat is defined as

$$C_V = T \left(\frac{\partial s}{\partial T} \right)_\mu. \quad (55)$$

The numerical results are displayed in the bottom panel of Fig. 3 for different values of the chemical potential. We can see that, when $\mu < \mu_c$ the specific heat has a negative branch and is multivalued, representing the unstable phase arising between $z_{\text{Min}} < z_h < z_{\text{Max}}$ in Fig. 1. In turn, for $\mu \geq \mu_c$ the specific heat is always positive, representing the stable black hole phase.

The speed of sound, which may be calculated from

$$c_s^2 = \frac{\partial \ln T}{\partial \ln s}, \quad (56)$$

is shown in the top panel of Fig. 4. Moreover, in the region where instabilities arise, $\mu < \mu_c$, c_s^2 becomes negative. This is related to the fact that the specific heat is multivalued and may have negative values,

$$c_s^2 = \frac{s}{C_V}. \quad (57)$$

For $\mu = \mu_c$, the square of the speed of sound touches the horizontal axis ($c_s^2 = 0$) at $T = T_c$. This fact is also related to the specific heat, which blows up at the critical temperature. Moreover, for $T < T_c$, c_s^2 increases rapidly. In turn, for $\mu > \mu_c$, it has a nonzero minimum at $T < T_c$. Finally, it is worth mentioning that in the high-temperature regime c_s^2 approaches asymptotically to the conformal value, $c_s^2 = 1/3$, in all the cases investigated here.

In the same way, we may calculate the susceptibility defined by

$$\chi = \left(\frac{\partial \rho}{\partial \mu} \right)_T. \quad (58)$$

The numerical results are displayed in the bottom panel of Fig. 4 for different values of the temperature. As can be seen, for $T < T_c$, $\rho(\mu)$ is a smooth monotonically increasing function (blue line), for $T = T_c$ (red line) there is a place where the susceptibility, i.e., the slope of the curve, blows up, which means that the susceptibility function has a singularity at $T = T_c$. Meanwhile, for $T > T_c$, there are two singularities at $\mu \neq \mu_c$, such that $\partial_\mu \rho$ blows up. Finally, as we have all the thermodynamic variables on hands we may calculate the trace anomaly, $\epsilon - 3p$. Our numerical results of the trace anomaly are displayed in the top panel of Fig. 5, where we plot it as a function of the temperature, as can be seen, there is a peak near to T_c , then, it decreases monotonically with the temperature. Whereas the maximum depends on the value of the chemical potential. As pointed out in Ref. [47], the behavior of the trace anomaly goes like $\sim 1/T^2$ for $T > T_c$, we also notice this behavior in the region of $T > T_c$, for small values of the chemical potential.

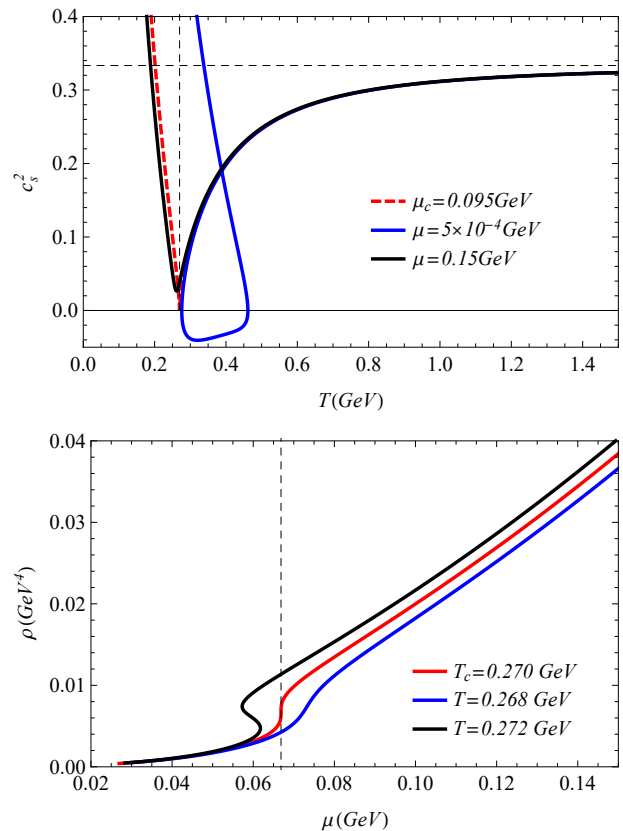


FIG. 4: Top: The figure shows the square of the speed of sound as a function of the temperature for different values of the chemical potential: $\mu < \mu_c$ (blue line), $\mu = \mu_c$ (red line) and $\mu_c < \mu$ (black line). Vertical dashed line represents $T = 0.270 \text{ GeV}$, while horizontal dashed line $c_s^2 = 1/3$. Bottom: The figure shows the baryons density as a functions of the chemical potential for different values of the temperature: $T < T_c$ (blue line), $T = T_c$ (red line) and $T_c < T$ (black line). Vertical dashed line represents $T = 0.270 \text{ GeV}$.

IV. PHASE DIAGRAM

Having described the thermodynamics and identified the critical point (μ_c, T_c) , now we may draw the phase diagram, which is obtained plotting the temperature as a function of the chemical potential. The phase diagram brings us information about the phase structure of the holographic model and shows the place where there are first-order, as well as the crossover phase transitions in the model we are working with. This diagram also shows the location of the critical point, which lies at the end of the first-order line transition. The numerical results are displayed in the bottom panel of Fig. 5, where the solid line represents the region of first-order phase transitions, this line finishes at the critical point (μ_c, T_c) , represented by the dark point, then, the phase transition becomes crossover, represented by the dashed line. These results are in agreement with a holographic model describing the heavy quarks system, as discussed in Ref. [33].

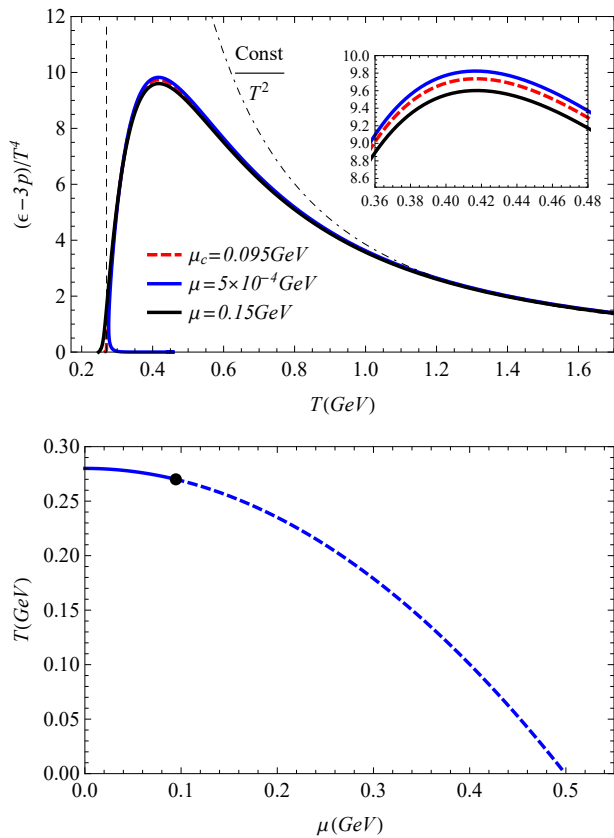


FIG. 5: Top: The figure shows the trace anomaly (or interaction measure) as a function of the temperature for different values of the chemical potential: for $\mu < \mu_c$ (blue line), $\mu = \mu_c$ (red line) and for $\mu_c < \mu$ (black line). Vertical line represents $T = 0.270\text{GeV}$, while the dotted dashed line the function Const/T^2 where $\text{Const} \approx 3.9$. Bottom: The phase diagram of the holographic model, solid line represents first-order phase transition, black dot point the critical point while dashed line crossover.

V. HOLOGRAPHIC COMPACT STARS

A. The heavy quarks zero temperature equation of state

So far we have fixed the parameter Λ using a critical temperature of about $T_c = 270$ MeV. However, in this section we relax this condition and let it to be a free parameter of the model. This will allow us to investigate the equation of state and compare the results against other models available in the literature, especially with those of Refs. [48, 53, 54]. The equation of state we are going to work with is given by Eq. (43), which was obtained from Eqs. (40) and (41). In the sequence, we follow the procedure implemented in Ref. [53], which was also followed in Ref. [48]. On the other hand, we fix the parameter Λ to get zero pressure at $\mu = 308.55$ MeV, which is the value of the chemical potential where the transition between the vacuum to nuclear and quark matter occurs. In our

model, the zero pressure condition provides a relation between Λ and μ , thus, from Eq. (40) we get

$$\Lambda = \frac{\mu}{\ell\sqrt{6}}, \quad (59)$$

from what follows $\Lambda = 125.965$ MeV.

A plot of the pressure as a function of the chemical potential is displayed in Fig. 6 in comparison to the results of the holographic model of Ref. [53], and also to the nuclear matter EoSs of Ref. [59]. In this figure, the heavy quark holographic EoS we are working with is plotted with a blue line, the nuclear matter EoSs results are plotted respectively with dashed green line (soft nuclear EoS), orange line (intermediate nuclear EoS), and by a dashed red line (stiff nuclear EoS), while the holographic EoS of Ref. [53] is represented by a cyan line. A matching procedure is implemented at the intersection point between the curve for the present holographic matter equation of state, cf. Eq. (42), and the curves for the nuclear matter EoSs. In this figure, the intersections are represented by black points, which are, respectively: $(\mu, p) = (440.272 \text{ MeV}, 103.679 \text{ MeV}/\text{fm}^3)$ for the stiff case, $(\mu, p) = (497.252 \text{ MeV}, 233.466 \text{ MeV}/\text{fm}^3)$ for the intermediate case, and $(\mu, p) = (597.255 \text{ MeV}, 662.592 \text{ MeV}/\text{fm}^3)$ for the soft EoS case.

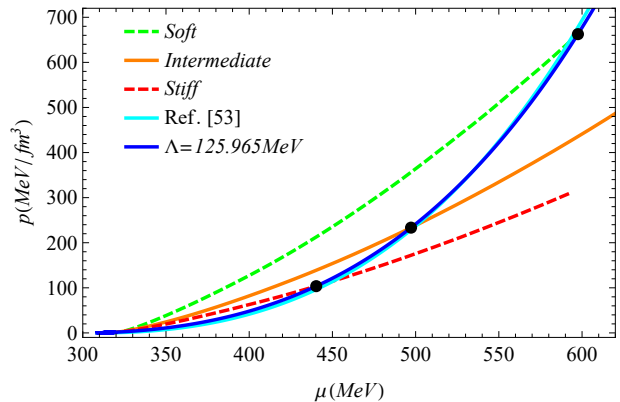


FIG. 6: The pressure as a function of the chemical potential for the holographic model (blue solid line) in comparison to the results of Ref. [53] (cyan solid line). In drawing this figure we have chosen $\Lambda = 125.965$ MeV (blue). The other lines represent the soft (dashed green), intermediate (solid orange), and stiff (dashed red) nuclear data of Ref. [59].

As seen in Fig. 6, the stiff matter EoS is dominant in the low densities region, then, a phase transition to the quark matter occurs at $\mu = 440.272$ MeV (at the intersection with the solid blue line). This means that the star has an outer structure dominated by the stiff nuclear matter, while its central region is dominated by the quark matter EoS. As pointed out in Ref. [53], it is expected a first-order phase transition from nuclear to quark matter. The same is valid for the transition from intermediate and soft nuclear matter EoSs to quark matter EoS. Compared to the top-down holographic model of Ref. [53] (solid cyan

line), the transitions occur at lower densities in the cases of stiff and intermediate EoSs. On the other hand, in the case of the soft EoS, the transition occurs at higher densities when compared to the results of Ref. [53].

We also explored the behavior of phase transitions for a fixed stiff hadronic EoS. For this objective we have considered different values of the parameter Λ , such that the transition from the hadronic to the quark matter phases occurs at higher densities. The results are displayed in Fig. 7, where the EoS of the holographic model is plotted for three different values of the parameter Λ , namely, 125.965 MeV (solid blue line), 133.372 MeV (solid black line), and 162.475 MeV (solid brown line). The stiff nuclear EoS from Ref. [59] is also drawn in such a figure (dashed red line). The intersections are represented by black points and have, respectively, the coordinates $(\mu, p) = (440.272 \text{ MeV}, 103.679 \text{ MeV}/\text{fm}^3)$ for the case with $\Lambda = 125.965 \text{ MeV}$ (solid blue line), $(\mu, p) = (469.714 \text{ MeV}, 137.653 \text{ MeV}/\text{fm}^3)$ for the case with $\Lambda = 133.373 \text{ MeV}$ (solid black line), and $(\mu, p) = (560.390 \text{ MeV}, 260.259 \text{ MeV}/\text{fm}^3)$ for the case with $\Lambda = 162.475 \text{ MeV}$ (solid brown line). It can be seen that an increase in the parameter Λ produces an increase in the transition pressure.

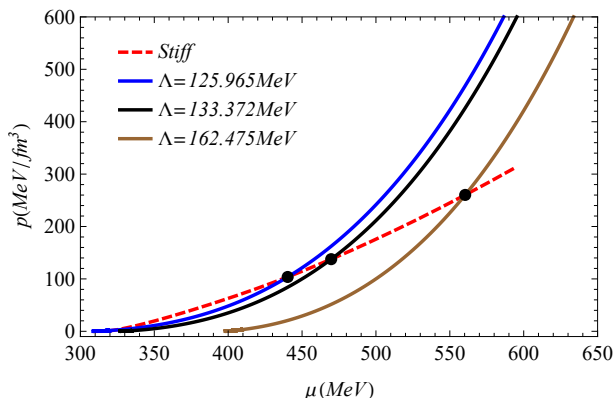


FIG. 7: The pressure as a function of the chemical potential of the holographic model for three different values of the parameter Λ . The dashed red line is the plot of the stiff nuclear EoS from Ref. [59].

B. Stellar structure of a heavy quark compact stars

This section is devoted to study the stellar structure of compact stars employing the equations of state discussed previously. In the sequence we choose geometrical units such that $G = 1 = c$. We consider the star as being composed of a perfect fluid whose energy-momentum tensor can be written in the form

$$T_{\mu\nu} = (\epsilon + p)u_\mu u_\nu + pg_{\mu\nu}, \quad (60)$$

with ϵ , p , and u_μ being respectively the energy density, the pressure, and the four-velocity of the fluid. In ad-

dition, for the generic background space-time of a static spherical star, we use the following line element

$$ds^2 = -e^{\nu(r)} dt^2 + e^{\lambda(r)} dr^2 + r^2(d\theta^2 + \sin^2\theta d\phi^2), \quad (61)$$

with (t, r, θ, φ) being Schwarzschild-like coordinates, and $\nu(r)$ and $\lambda(r)$ are functions of the indicated coordinate alone. The Einstein equations in such a spacetime lead to the well known Tolman-Oppenheimer-Volkov equations for stellar structure,

$$\frac{dp}{dr} = -\frac{\epsilon m}{r^2} \left(1 + \frac{p}{\epsilon}\right) \left(1 + \frac{4\pi p r^3}{m}\right) \left(1 - \frac{2m}{r}\right)^{-1}, \quad (62)$$

$$\frac{d\nu}{dr} = -\frac{2}{\epsilon} \frac{dp}{dr} \left(1 + \frac{p}{\epsilon}\right)^{-1}, \quad (63)$$

$$\frac{dm}{dr} = 4\pi r^2 \epsilon, \quad (64)$$

where m , p , and ϵ , and ν are function of the radius r only. The integration of these equations requires initial conditions. As usual, we take $P(r=0) = p_c$ as the given central pressure, $m(r=0) = 0$ and $\nu(r=0) = \nu_c$ as a given value for the metric field at the center of the star. During integration, we also use the equation of state to obtain the energy density ϵ at each radius r inside the star. We finish the integration when the pressure reaches the zero value. At this point we identify the coordinate $r = R$ as the star radius and $M = m(R)$ as the star mass. In the cases of one phase hadronic stars we use the procedure described above but in the cases of two-phases stars (hybrid stars) we use two separated numerical integrations inside the star. The first one is the integration from the center to the interface (i.e., the place where the pressures reach its transition value), and the second one is the integration from the interface to the surface of the star. In Fig. 8 we show the evolution of the normalized energy density (in terms of the central density ϵ_c), and of the normalized pressure (in terms of the central pressure p_c) across a particular star described by the quark matter (solid line) and nuclear stiff (dotted line) EoSs. As it can be seen, the energy density is discontinuous at the interface between the two matter phases. The pressure is continuous but its derivative is not defined at the interface.

The numerical results for the mass of the compact objects as a function of the respective radius are displayed in Fig. 9. We come up with stellar models composed of hadronic matter and quark matter, the so called hybrid stars. Before phase transition pure hadronic stars are obtained and they correspond to red dashed, orange and green dashed lines, those stars were build using the stiff, intermediate and soft EoS respectively. Black lines represent hybrid stars composed of nuclear and quark matter. As we can observe, this scenario supports stars with masses of $2.44M_\odot$, $2.29M_\odot$ and $2.00M_\odot$, respectively. The corresponding radii are 14.3 km, 12.2 km, and 9.57 km, respectively. It can be seen that these so-

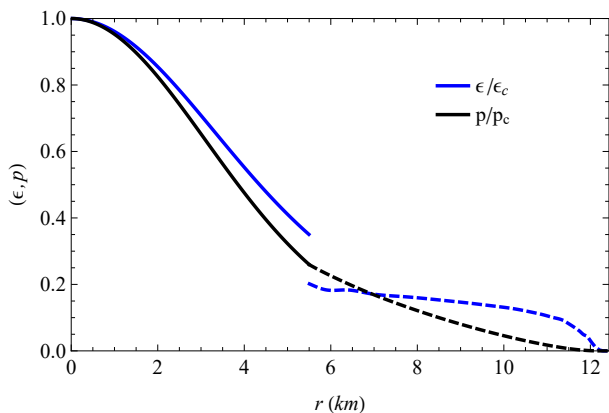


FIG. 8: The figure shows the evolution of the normalized energy density (blue) and normalized pressure (black) as a function of the radius in the interior of a single star. The quark matter EoS is represented by solid lines, while the stiff nuclear EoS by dashed lines. To get this figure we have fixed the central pressure in $400 \text{ MeV}/\text{fm}^3$ and $\Lambda = 125.965 \text{ MeV}$.

lutions are unstable under the static criterion of stability [60] (see also [61]).

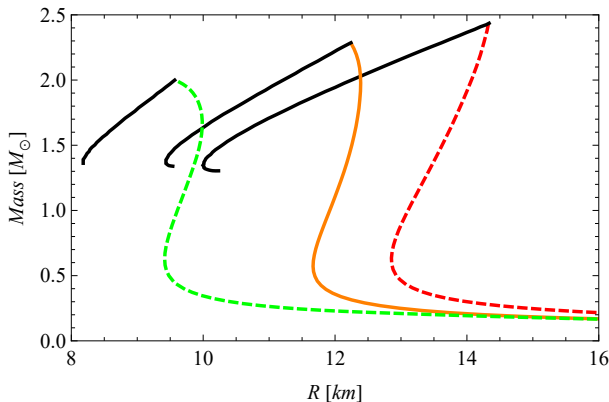


FIG. 9: The figure shows the mass-radius relation of the holographic model we are working with (black lines), while the colored lines represent the nuclear EoS plotted in Fig 6.

Finally, we solve the TOV equations for the EoSs displayed in Fig. 7 in order to obtain the mass-radius relation for hybrid stars, and the results are displayed in Fig. 10. We observe that the maximum mass depends on the transition point, the larger the chemical potential (and pressure) the larger the mass of the star. Thus, the maximum masses are: $2.42M_\odot$, $2.61M_\odot$ and $2.87M_\odot$ for $\Lambda = 125.965 \text{ MeV}$, $\Lambda = 133.372 \text{ MeV}$ and $\Lambda = 162.475 \text{ MeV}$, respectively. It is worth pointing out that these results are qualitatively equivalent to the results presented in Ref. [48].

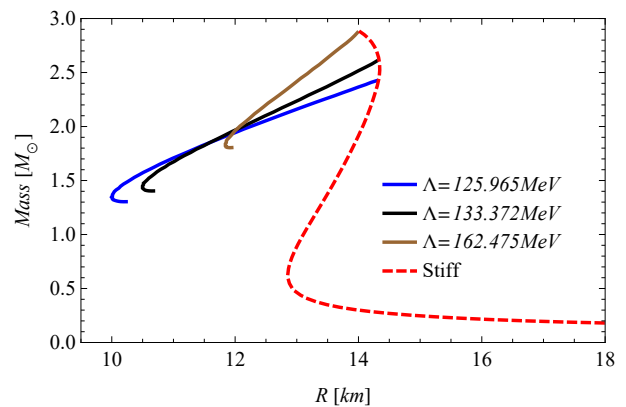


FIG. 10: The figure shows the mass-radius relation of the present holographic model corresponding to the EoSs displayed in Fig. 7

VI. CONCLUSION AND OUTLOOK

The thermodynamics and the phase structure of heavy quarks systems were studied in this work by using the holographic description. The interpretation of our results are motivated by a previous holographic model investigated in [33], where the phase diagram is in agreement with a system composed by heavy quarks when contrasted with lattice QCD results. The holographic model used in this work was implemented in the context of Einstein-Maxwell-Dilaton theories. Its dual quantum field theory is at finite temperature and density. We show that the thermodynamic properties are sensitive to the value of chemical potential.

We found a first-order phase transition for $\mu < \mu_c$ and also showed that the critical point lies at $\mu = \mu_c$, where the phase transition becomes second-order. In turn, for $\mu > \mu_c$ the transitions become crossover. The phase diagram summarises these findings.

On the other hand, to investigate the inner structure of compact objects, we realized that the expression of the free energy naturally decouples, allowing us to get an expression, which is independent of the temperature. This expression allows us to calculate the equation of state and investigate the inner structure of stars composed by heavy quarks with a nuclear matter outer crust through a matching procedure. Analogously to what was done in [53] (see also [54]), we explore the transition between the nuclear matter EoSs to quark matter EoS. It is worth mentioning that the equation of state we got is qualitatively equivalent to the one obtained in the holographic top-down approach investigated in [53, 54]. Indeed, the results of the pressure as a function of the chemical potential are quantitatively equivalents, showing the consistency of the top-down and bottom-up approaches for describing QCD-like theories. We conclude that in all cases the quark matter stars we found are unstable.

Finally, we stress that the present study of a bottom-up holographic model is the first step and we will expand

it to investigate more realistic equations of state, which will be useful in order to describe the inner structure of compact objects, resulting in important applications in Astrophysics. We are also planning to address further studies, turning on the kinetic function, which allows us to get a phase diagram in agreement with the one expected in QCD [34]. Other directions of investigation also include the use of the holographic dictionary to include magnetic field [62] and nucleons in the theory to model the matter inside compact objects.

Acknowledgments

We would like to thank Jorge Noronha, Romulo Rougemont and Alfonso Ballon Bayona for stimulating discussions along the development of this work. L. A. H. M. and V. T. Z. thank financial support from Coordenação de Aperfeiçoamento de Pessoal de Nível Superior (CAPES, Brazil), Programa Nacional de Pós-Doutorado, and Grant No. 88881.310352/2018-01. V. T. Z. also thanks financial support from Conselho Nacional de Desenvolvimento Científico e Tecnológico (CNPq, Brazil), Grant No. 309609/2018-6.

Appendix A: Equation of state in AdS Einstein-Maxwell solution

In this section, we investigate the extremal solution of the Einstein-Maxwell equations. In this case, the solution of the gauge field is given by

$$A_0(z) = \mu - Qz^2. \quad (\text{A1})$$

The condition at the horizon gives us $Q = \mu/z_h^2$. It is worth mentioning that the relation (14) reduces to this result when Λ goes to zero. While the horizon function solution is given by Eq. (20). Then, the black hole temperature is

$$T = \frac{1}{z_h \pi} \left(1 - \frac{q^2 z_h^6}{2} \right). \quad (\text{A2})$$

We also may calculate the entropy density using the relation (29)

$$s = \frac{2\pi\ell^3}{\kappa^2 z_h^3}. \quad (\text{A3})$$

In the same way the free energy through (32)

$$\mathcal{F} = -\frac{\ell^2}{2\kappa^2 z_h^4} - \frac{5\ell\mu^2}{6\kappa^2 z_h^2}. \quad (\text{A4})$$

Analogously, the pressure is $p = -\mathcal{F}$

$$p = \frac{\ell^2}{2\kappa^2 z_h^4} + \frac{5\ell\mu^2}{6\kappa^2 z_h^2}. \quad (\text{A5})$$

Let us consider the relationship between the charge and the chemical potential, which is obtained plugging evaluating Eq. (A1) at the horizon, then, plugging $Q = \mu/z_h^2$ in Eq. (19) we get

$$q^2 = \frac{\mu^2}{3z_h^4 \ell^2}. \quad (\text{A6})$$

Then, we may write the temperature (A2) as a function of the chemical potential

$$T = \frac{1}{\pi z_h} \left(1 - \frac{z_h^2 \mu^2}{6\ell^2} \right). \quad (\text{A7})$$

The last equation is a quadratic equation on z_h . Solving this equation we get a relation of z_h as a function of the temperature and chemical potential

$$z_h = \frac{-3\pi T \ell^2 + \ell (9\pi^2 T^2 \ell^2 + 6\mu^2)^{1/2}}{\mu^2}. \quad (\text{A8})$$

Expanding the square root in the high temperature regime, keeping up to the first subleading term we get

$$z_h = \frac{1}{\pi T} - \frac{\mu^2}{6\pi^3 \ell^2 T^3} + \mathcal{O}(1/T^5) \quad (\text{A9})$$

Plugging (A9) and κ from (A2) in (A3), then, we expand in the high temperature regime, the asymptotic expression for the entropy becomes

$$s = \frac{2\pi^4 \ell^3 T^3}{\kappa^2} + \frac{\pi^2 \ell \mu^2 T}{\kappa^2} + \mathcal{O}(\mu^4/T, \mu^6/T^3) \quad (\text{A10})$$

we observe that the entropy scales correctly with the temperature. In turn, plugging (A8) in (A4) the free energy is given by

$$\mathcal{F} = -\frac{\pi^4 \ell^3 T^4}{2\kappa^2} - \frac{7\pi^2 \ell \mu^2 T^2}{6\kappa^2} - \frac{11\mu^4}{36\ell\kappa^2} + \mathcal{O}(\mu^6/T^2), \quad (\text{A11})$$

where $\mathcal{O}(\mu^6/T^2)$ contains higher-order contributions. Observing Eq. (A11) the expression decouples into one piece depending only on the temperature, chemical potential and a mixture of the form $\mathcal{O}(\mu^6/T^2)$. The pressure is given by $p = -\mathcal{F}$, therefore, the pressure also decouples. Considering the piece depending only on the chemical potential, because we want to describe a cold phase in the dual field theory, we get

$$p = \frac{11\mu^4}{36\ell\kappa^2}, \quad (\text{A12})$$

whereas the energy density is given by

$$\epsilon = \frac{11\mu^4}{12\ell\kappa^2}. \quad (\text{A13})$$

Hence, the equation of state is $\epsilon = 3p$, which is the equation of state of a system preserving conformal symmetry.

On the other hand, let us investigate the extremal solution of the Reissner-Nordstrom AdS solution, which is

given when the temperature (A2) vanishes, it happens when $q = \sqrt{2}/z_h^3$. It is worth mentioning that the location z_h can be chosen close to the boundary, this means that the value of the black hole charge should be large. Plugging $Q = \mu/z_h^2$ and $q = \sqrt{2}/z_h^3$ in (19) we get a relation between μ and z_h

$$z_h = \frac{\sqrt{6}\ell}{\mu}. \quad (\text{A14})$$

Then, plugging q and z_h in (A3), (A3) and (A5) we get

$$s = \frac{\pi\mu^3}{3\sqrt{6}\kappa^2}, \quad \mathcal{F} = -\frac{\mu^4}{12\kappa^2\ell}, \quad p = \frac{\mu^4}{12\kappa^2\ell}. \quad (\text{A15})$$

Now, we may calculate the energy density using the relation $\epsilon = \mu \partial_\mu p - p$, which gives us

$$\epsilon = \frac{\mu^4}{4\kappa^2\ell}. \quad (\text{A16})$$

Finally, the equation of state of the extremal solution is

$$\epsilon = 3p, \quad (\text{A17})$$

which is the equation of state of a system preserving conformal symmetry. It is worth mentioning that in the extremal solution we do not do any approximation.

Finally, let us write the metric in the extremal case and expand it close to the horizon. Plugging $q = \sqrt{2}/z_h^3$

in (20)

$$f(z) = (z^2 - z_h^2)^2 \frac{(2z^2 + z_h^2)}{zh^6}, \quad (\text{A18})$$

then,

$$f(\tilde{z}) \approx 12 \frac{\tilde{z}^2}{z_h^2} + 28 \frac{\tilde{z}^3}{z_h^3} + \mathcal{O}(\tilde{z}^4/z_h^4), \quad (\text{A19})$$

where we have defined $\tilde{z} = z - z_h$. Plugging this result in the metric (6) and $A = -\ln(z/\ell)$

$$ds^2 = -12 \frac{\ell^2 \tilde{z}^2}{z_h^4} dt^2 + \frac{\ell^2}{12\tilde{z}^2} d\tilde{z}^2 + \frac{\ell^2}{z_h^2} dx_i dx^i. \quad (\text{A20})$$

Defining the variable $\hat{r} = \tilde{z} z_h^2 / \ell^2$, the metric becomes

$$ds^2 = -12 \frac{\hat{r}^2}{\ell^2} dt^2 + \frac{\ell^2}{12\hat{r}^2} d\hat{r}^2 + \frac{\ell^2}{z_h^2} dx_i dx^i. \quad (\text{A21})$$

This is the $AdS_2 \times \mathbb{R}^3$ metric, with boundary at $\hat{r} \rightarrow \infty$ and radius $\ell = \ell/\sqrt{12}$. The emergence of this geometry in the IR is related to the emergence of quantum criticality arising naturally in the holographic model, for details see Ref. [57].

-
- [1] O. Philipsen, arXiv:1009.4089 [hep-lat].
- [2] F. Karsch, PoS CPOD **07**, 026 (2007) [arXiv:0711.0656 [hep-lat]].
- [3] H. Satz, Lect. Notes Phys. **785**, 1 (2010) [arXiv:0803.1611 [hep-ph]].
- [4] C. R. Stephens, G. 't Hooft and B. F. Whiting, Class. Quant. Grav. **11**, 621 (1994) [gr-qc/9310006].
- [5] L. Susskind, J. Math. Phys. **36**, 6377 (1995) [hep-th/9409089].
- [6] J. M. Maldacena, Int. J. Theor. Phys. **38**, 1113 (1999) [Adv. Theor. Math. Phys. **2**, 231 (1998)] [hep-th/9711200].
- [7] S. S. Gubser, I. R. Klebanov and A. M. Polyakov, Phys. Lett. B **428**, 105 (1998) [hep-th/9802109].
- [8] E. Witten, Adv. Theor. Math. Phys. **2**, 253 (1998) [hep-th/9802150].
- [9] A. Karch and E. Katz, JHEP **0206**, 043 (2002) [hep-th/0205236].
- [10] T. Sakai and S. Sugimoto, Prog. Theor. Phys. **113**, 843 (2005) doi:10.1143/PTP.113.843 [hep-th/0412141].
- [11] T. Sakai and S. Sugimoto, Prog. Theor. Phys. **114**, 1083 (2005) doi:10.1143/PTP.114.1083 [hep-th/0507073].
- [12] J. Erlich, E. Katz, D. T. Son and M. A. Stephanov, Phys. Rev. Lett. **95**, 261602 (2005). [hep-ph/0501128].
- [13] A. Karch, E. Katz, D. T. Son and M. A. Stephanov, Phys. Rev. D **74**, 015005 (2006). [hep-ph/0602229].
- [14] S. J. Brodsky and G. F. de Téramond, Phys. Lett. B **582** (2004), 211-221 [arXiv:hep-th/0310227 [hep-th]].
- [15] C. Csaki and M. Reece, JHEP **0705**, 062 (2007) [hep-ph/0608266].
- [16] U. Gursoy and E. Kiritsis, JHEP **0802**, 032 (2008) [arXiv:0707.1324 [hep-th]].
- [17] U. Gursoy, E. Kiritsis and F. Nitti, JHEP **0802**, 019 (2008). [arXiv:0707.1349 [hep-th]].
- [18] B. Batell and T. Gherghetta, Phys. Rev. D **78**, 026002 (2008) [arXiv:0801.4383 [hep-ph]].
- [19] W. de Paula, T. Frederico, H. Forkel and M. Beyer, Phys. Rev. D **79**, 075019 (2009) [arXiv:0806.3830 [hep-ph]].
- [20] D. Li and M. Huang, JHEP **11** (2013), 088 [arXiv:1303.6929 [hep-ph]].
- [21] A. Ballon-Bayona, H. Boschi-Filho, L. A. H. Mamani, A. S. Miranda and V. T. Zanchin, Phys. Rev. D **97**, no. 4, 046001 (2018).
- [22] L. A. H. Mamani, Phys. Rev. D **100**, no. 10, 106009 (2019) [arXiv:1910.00026 [hep-th]].
- [23] S. S. Gubser and A. Nellore, Phys. Rev. D **78**, 086007 (2008) [arXiv:0804.0434 [hep-th]].
- [24] S. S. Gubser, A. Nellore, S. S. Pufu and F. D. Rocha, Phys. Rev. Lett. **101**, 131601 (2008) [arXiv:0804.1950 [hep-th]].
- [25] U. Gursoy, E. Kiritsis, L. Mazzanti and F. Nitti, Phys. Rev. Lett. **101**, 181601 (2008) [arXiv:0804.0899 [hep-th]].
- [26] U. Gursoy, E. Kiritsis, L. Mazzanti and F. Nitti, JHEP **0905**, 033 (2009) [arXiv:0812.0792 [hep-th]].
- [27] U. Gursoy, E. Kiritsis, L. Mazzanti and F. Nitti, Nucl. Phys. B **820**, 148 (2009) [arXiv:0903.2859 [hep-th]].

- [28] U. Gursoy, E. Kiritsis, G. Michalogiorgakis and F. Nitti, *JHEP* **0912**, 056 (2009) [arXiv:0906.1890 [hep-ph]].
- [29] J. Noronha, *Phys. Rev. D* **81**, 045011 (2010) [arXiv:0910.1261 [hep-th]].
- [30] O. DeWolfe, S. S. Gubser and C. Rosen, *Phys. Rev. D* **83**, 086005 (2011).
- [31] O. DeWolfe, S. S. Gubser and C. Rosen, *Phys. Rev. D* **84**, 126014 (2011) doi:10.1103/PhysRevD.84.126014 [arXiv:1108.2029 [hep-th]].
- [32] R. G. Cai, S. He and D. Li, *JHEP* **1203**, 033 (2012) [arXiv:1201.0820 [hep-th]].
- [33] S. He, S. Y. Wu, Y. Yang and P. H. Yuan, *JHEP* **1304**, 093 (2013) [arXiv:1301.0385 [hep-th]].
- [34] Y. Yang and P. H. Yuan, *JHEP* **1411**, 149 (2014) [arXiv:1406.1865 [hep-th]].
- [35] S. I. Finazzo, R. Rougemont, M. Zaniboni, R. Critelli and J. Noronha, *JHEP* **1701**, 137 (2017) [arXiv:1610.01519 [hep-th]].
- [36] J. Knaute, R. Yaresko and B. Kämpfer, *Phys. Lett. B* **778**, 419 (2018) [arXiv:1702.06731 [hep-ph]].
- [37] Z. Li, Y. Chen, D. Li and M. Huang, *Chin. Phys. C* **42**, no. 1, 013103 (2018) [arXiv:1706.02238 [hep-ph]].
- [38] S. J. Sin, *JHEP* **0710**, 078 (2007).
- [39] P. Colangelo, F. Giannuzzi and S. Nicotri, *Phys. Rev. D* **83**, 035015 (2011) [arXiv:1008.3116 [hep-ph]].
- [40] B. H. Lee, C. Park and S. J. Sin, *JHEP* **0907**, 087 (2009).
- [41] C. Park, *Phys. Rev. D* **81**, 045009 (2010).
- [42] C. Park, D. Y. Gwak, B. H. Lee, Y. Ko and S. Shin, *Phys. Rev. D* **84**, no. 4, 046007 (2011) Erratum: [*Phys. Rev. D* **90**, no. 12, 129902 (2014)].
- [43] P. Colangelo, F. Giannuzzi, S. Nicotri and V. Tangorra, *Eur. Phys. J. C* **72**, 2096 (2012) [arXiv:1112.4402 [hep-ph]].
- [44] B. P. Abbott *et al.* *Phys. Rev. Lett.* **119**, no. 16, 161101 (2017) [arXiv:1710.05832 [gr-qc]].
- [45] R. C. Tolman, *Phys. Rev.* **55**, 364 (1939).
- [46] J. R. Oppenheimer and G. W. and Volkoff, *Phys. Rev.* **55**, 374 (1939).
- [47] M. Caselle, L. Castagnini, A. Feo, F. Gliozzi, U. Gursoy, M. Panero and A. Schafer, *JHEP* **1205**, 135 (2012).
- [48] K. Bitaghsir Fadafan, J. Cruz Rojas and N. Evans, [arXiv:1911.12705 [hep-ph]].
- [49] C. Ecker, M. Järvinen, G. Nijs and W. van der Schee, [arXiv:1908.03213 [astro-ph.HE]].
- [50] P. M. Chesler, N. Jokela, A. Loeb and A. Vuorinen, *Phys. Rev. D* **100** (2019) no.6, 066027 [arXiv:1906.08440 [astro-ph.HE]].
- [51] K. Zhang, T. Hirayama, L. Luo and F. Lin, *Phys. Lett. B* **801** (2020), 135176 [arXiv:1902.08477 [hep-ph]].
- [52] N. Jokela, M. Järvinen and J. Remes, *JHEP* **03** (2019), 041 [arXiv:1809.07770 [hep-ph]].
- [53] C. Hoyos, D. Rodríguez Fernández, N. Jokela and A. Vuorinen, *Phys. Rev. Lett.* **117**, no. 3, 032501 (2016) [arXiv:1603.02943 [hep-ph]].
- [54] E. Annala, C. Ecker, C. Hoyos, N. Jokela, D. Rodríguez Fernández and A. Vuorinen, *JHEP* **1812**, 078 (2018) [arXiv:1711.06244 [astro-ph.HE]].
- [55] C. Hoyos, N. Jokela, M. Jarvinen, J. G. Subils, J. Tarrío and A. Vuorinen, [arXiv:2005.14205 [hep-th]].
- [56] N. Jokela, M. Jarvinen, G. Nijs and J. Remes, [arXiv:2006.01141 [hep-ph]].
- [57] T. Faulkner, H. Liu, J. McGreevy and D. Vegh, *Phys. Rev. D* **83** (2011), 125002 [arXiv:0907.2694 [hep-th]].
- [58] M. Alford, M. Braby, M. Paris and S. Reddy, *Astrophys. J.* **629** (2005), 969-978 doi:10.1086/430902 [arXiv:nucl-th/0411016 [nucl-th]].
- [59] K. Hebeler, J. Lattimer, C. Pethick and A. Schwenk, *Astrophys. J.* **773** (2013), 11 [arXiv:1303.4662 [astro-ph.SR]].
- [60] J. P. Pereira, C. V. Flores and G. Lugones, *Astrophys. J.* **860** (2018) no.1, 12 [arXiv:1706.09371 [gr-qc]].
- [61] N. Glendenning, *Compact stars: Nuclear physics, particle physics, and general relativity*, (Springer-Verlag New York., 1996) p. 91.
- [62] S. He, Y. Yang and P. H. Yuan, [arXiv:2004.01965 [hep-th]].